CHAPTER 2

EXPERIMENTAL DETAILS

EXPERIMENTAL DETAILS

2.1 Introduction

Nanostructured materials are gaining research interest to science and technology because of their anomalous characteristics which differ significantly from their bulk counterparts. Nanostructured materials are classified as those which have at least one dimension in the 1-100 nm range. Materials in this size domain exhibit interesting properties, for example, nanocrystals possesses a very low melting point, reduced lattice constants, thermal stability etc. However, to realize the novel physical properties and potential applications, the foremost challenge is the fabrication of nanostructured materials. Different approaches and techniques are explored for the synthesis of nanomaterials which are broadly classified into two categories: top-down methods and bottom-up approaches [1-4]. The top-down approaches involve various methods viz., high energy ball milling, wire explosion, arc discharge, inert gas condensation, laser ablation, ion sputtering etc. In the bottom-up methods, a varied range of techniques is used such as chemical reduction, electrochemical synthesis, arrested precipitation, solvothermal synthesis, photochemical synthesis etc. [5-9]. In this thesis, we have adopted a bottom-up approach for the development of different nanosystems. The bottom-up synthesis approach was preferred in our work due to its better control over the properties of the nanosystems.

Nanoparticles with controlled morphology and engineered properties are an absolute requisite for their applications in biomedical technology [10-14]. Also, for biomedical applications, the nanoparticles have to be hydrophilic and stable in biological media. Direct synthesis of hydrophilic nanostructures is a challenge and hence many strategies are being used for the surface modification of hydrophobic nanostructures to hydrophilic nanostructures.

2.2 Synthesis of hydrophobic nanoparticles and surface modification

As mentioned earlier, for any biomedical applications the nanoparticles have to be hydrophilic, selective towards specific targets and compatible with the biological

species. In addition to that, the nanoparticles have to be monodisperse and uniform in size so that each nanoparticle has nearly similar physical and chemical properties. Now, it is noteworthy to mention that the most suitable for making monodisperse and shape controlled nanoparticles are through non-hydrolytic approaches [15-20]. As a consequence, nanoparticles synthesized using such media are highly hydrophobic in nature and are dispersed only in selected organic solvents. Also, in case of some toxic metal-based nanoparticles, their surfaces are passivated using silica or other coatings which can prevent the oxidation of the core metal nanoparticles. Moreover, most of the monodisperse magnetic metal oxide nanoparticles developed through the nonhydrolytic routes is capped with surfactants for controlled morphology. As a result, these surfactants are generally hydrophobic which in turn makes the nanoparticles strongly hydrophobic in nature. Furthermore, in case of magnetic nanoparticles, an inert coating is required that can prevent aggregation of the nanoparticles. But, such nanoparticles cannot be readily employed in biological systems which otherwise require hydrophilic environments.

To make these hydrophobic nanostructures suitable for biomedical applications, various strategies are used for their surface modification. Ligand exchange is the most versatile approach for replacing the hydrophobic coating of the nanoparticles with hydrophilic molecules [21-27]. In the ligand exchange method, an excess of ligand is added to the nanoparticle solution to displace the original ligand on a nanoparticles surface.

2.3 Direct synthesis of hydrophilic nanoparticles

For the surface engineering of hydrophobic nanoparticles, post-synthesis exchange process of surface bound ligands on nanoparticles still appears to be the most acceptable and widely used. However, this strategy is very long and tedious. Therefore, it is interesting to explore if hydrophilic nanoparticles can be synthesized directly. Some recent reports suggest the direct synthesis of hydrophilic nanoparticles [28-34]. However, it is challenging to maintain the specific property of nanosystem through one-pot hydrophilic synthesis routes. The polyol method is a versatile chemical approach, where metal salts are reduced to metal particles in presence of suitable polyols (for example ethylene glycol, diethylene glycol) and has been successfully used to prepare a

large variety of non-aggregated inorganic nanoparticles. Polyols used in this method work as a high-boiling solvent and reducing agent, as well as a stabilizer to control the growth of the particles and also prevent interparticle aggregation. The most important advantage of this method is that direct synthesis of hydrophilic nanoparticles is possible without the use of any reducing agent or surfactants. Also, there is the possibility to kinetically control the experimental conditions and easily scale-up for mass production of hydrophilic nanoparticles. However, in this method proper selection of polyol is important for the efficient growth of the nanoparticles and their solubility. The nanoparticles prepared using the polyol approach is intrinsically stabilized with a layer of hydrophilic polyol molecules and as a result they exhibit long-term stability in aqueous media without the need of any surface modification.

2.4 Analytical techniques

Different analytical techniques were employed for characterization of the nanosystems studied in this thesis.

1. ***X-ray Diffraction*:** Powder XRD technique was employed to characterize all nanoparticle samples synthesized in this thesis, as the samples were in powder form. Powder XRD must be used for the polycrystalline samples because it allows the possible crystal orientations to be accessed simultaneously. The XRD is a valid method for determining the degree of crystallinity of a sample as well as to know the crystal structure. The spacing of various peaks also gives the information for determining the lattice parameters. As the size of the nanocrystals decrease, the line width is broadened due to loss of long-range order relative to the bulk. All powder XRD measurements were done using the X-ray diffractometer (Rigaku) with Cu $K_{\breve{U}}$ radiation (∂ = 1.54056 Å) to elucidate the phase of different types of nanosystems.

2. ***UV-Visible Absorption Spectroscopy*:** The optical absorption properties of nanosystems were studied by UV-Visible absorption spectrophotometer (Shimadzu, UV-2450). The characterization of samples was done using Quartz cuvette. The samples were characterized in liquid form at room temperature.

3. ***PL Spectroscopy*:** The optical emission properties of nanosystems were measured by PL spectrophotometer (Perkin Elmer, LS55). The characterization of samples was done using Quartz cuvette. The samples were characterized in liquid form at room temperature. The concentration of samples was same in both UV-vis and PL spectroscopy.

4. ***Fourier Transform Infra-red Spectroscopy*:** The surface functionalities of the nanosystems were examined by FTIR spectroscopy (Nicolet Impact I-410). It is a technique that can provide very useful information about functional groups present on the surface of a sample. An infrared spectrum represents the fingerprint of a sample with absorption peaks which correspond to the frequencies of vibrations between the bonds of the atoms. Because each different material is a unique combination of atoms. Hence, no two compounds produce the exactly same infrared spectrum. For the FTIR measurements, powdered samples were mixed with KBr powder and pelletized. The background correction was made using a reference blank of KBr pellet.

5. ***Transmission Electron Microscopy*:** The nanosystems were imaged in 200 kV JEOL JEM- 2200FS Transmission Electron Microscope (TEM) to determine the average particle size, morphology, and associated selected area diffraction (SAED) method. Samples were typically prepared from a dilute solution of nanoparticles in suspension. A drop of the solution was put on the HR-TEM sample holder (carbon-coated copper grid, 300-mesh) and allowed to evaporate. The desired result is a single/multiple layers of nanoparticles. This technique is useful as a direct measurement of size and shapes of nanoparticles.

6. ***EDX Spectroscopy*:** This is a powerful and useful tool for elemental analysis. X-ray microanalysis in the electron microscope is the process of using characteristic X-rays, generated in a specimen by the electron beam, to determine the element composition of the specimen. Five different areas were chosen for confirming the stoichiometry of each sample. The compositional characterizations of magnetic, QDs and hybrid nanosystems were carried out with energy dispersive X-ray microanalysis (EDX 7582, Oxford Instrument, UK).

7. ***Physical Properties Measurement System (PPMS)*:** The magnetic characterizations of magnetic nanosystems were done with vibrating sample magnetometer (VSM). The system used for this research has temperature capabilities of 5-300 K and uses a liquid-helium cooled superconducting magnet that can attain magnetic fields up to 9 Tesla.

8. ***Fluorescence Microscopy*:** The fluorescence images of nanosystems were taken by inverted fluorescence microscope (LEICA DMI6000B). The conventional microscope produces a magnified image of a specimen under illumination of visible light (400-700 nanometers). On the other hand, a fluorescence microscope uses a much higher intensity light source which excites a fluorescent species in a specimen of interest. This fluorescent specimen in turn emits a lower energy light of a longer wavelength that produces the magnified image irrespective of the incident light. We used a Mercury arc-discharge lamp for more intense light. In our case, the fluorescent material is quantum dots (QDs) and hybrid nanosystems (HNs). The cellular uptake of the QDs and HNs were examined under the fluorescence microscope.

9. ***Thermogravimetric Analysis*:** This study was carried out for powder samples (approx 3 mg) with a heating rate of 10 °C/min using a Shimadzu TGA 50 thermogravimetric analyzer in N_2 atmosphere up to ~ 600°C.

10. ***Contrast Property Characterization:*** The transverse relaxation time for the MRI contrast properties of the NPs were measured using 14.1T, Nuclear magnetic resonance (NMR) micro imager (Bruker AVANCE). For evaluation of the contrast properties of magnetic and magneto-fluorescent hybrids NPs, the transverse relaxivity of the NPs was evaluated by measuring the transverse relaxation time (T_2) of water in the presence of different amount of test samples. The transverse relaxation time (T_2) of water was measured at 25 $^{\circ}$C using spin echo sequence at 14.1 T magnet interface with micro imager system.

11. ***ICP-OES*:** ICP-OES stands for Inductively Coupled Plasma Optical Emission Spectrometry. The sample was introduced into the ICP in liquid form. It is based on Atomic Emission Spectroscopy, where the sample in plasma state at high temperature (up to 8000 Kelvin) was converted to free, excited or ionized ions. The excited atom emits a radiation(s) when it goes back to the ground state. The emitted characteristic radiations and intensities were measured optically by detectors. The trace metal concentration of aqueous solutions of the samples was analyzed using inductively coupled plasma (ICP) mass spectrometry (Perkin Elmer). The concentration of Fe atom was required for the measurement of relaxivity of different nanosystems. The concentration of different metals for analysis of toxicity was also calculated using ICP-OES.

12. ***X-ray Photoelectron Spectroscopy*:** X-ray photoelectron spectroscopy (XPS) studies were executed to obtain information on the coating the surface of nanosystems. Monochromatic Al $K_{\check{U}}$ ($h_{\check{z}}$ = 1486.6 eV) X-rays was used to eject core electrons from the sample at 45° take-off angle. High-resolution scans of a peak can be used to distinguish among species of the same element. The photoelectrons ejected from the material are detected and their energies measured. Calibration of the binding energy (BE) of the measured spectra was performed at the C1s peak of the adsorbed hydrocarbons (BE= 285 eV) as an internal reference. Gaussian peak profiles were used for the deconvolution of XPS spectra.

13. **Zeta potential analyzer:** Zeta potential is a physical property which is demonstrated by the particles in suspension. Zeta potential is a measure of the magnitude of the electrostatic or charge repulsion/attraction between particles and is one of the fundamental parameters known to affect the stability of systems. The magnitude of the zeta potential gives an indication of the potential stability of the colloidal system. If all the particles in suspension have a large negative or positive zeta potential then they will tend to repel each other and there will be the least tendency for the particles to come together. However, if the particles have low zeta potential values then there will be a weak force to prevent the particles coming together and aggregated. The dividing line between stable and unstable suspensions

is generally taken at either ±30 mV. Particles with zeta potentials more positive than +30 mV or more negative than -30 mV are normally considered stable.

In aqueous media, the pH of the sample is one of the most important factors that affects its zeta potential. A zeta potential value on its own without defining the solution conditions is virtually a meaningless number. Suppose a particle is in suspension with a negative zeta potential. If more alkali is added to this suspension then the particles tend to acquire the more negative charge. If acid is added to this suspension then a point will be reached where the charge will be neutralized. Further addition of acid will cause a build-up of positive charge. Therefore, a zeta potential versus pH curve will be positive at low pH and lower or negative at high pH. There may be a point where the plot passes through zero zeta potential. This point is called the isoelectric point and is very important from a practical consideration. It is normally the point where the colloidal system is least stable. Samples were characterized with Micromeretics Nanoplus-3 in a liquid state.

2.5 Definition of key terms

a) Zero-field cooling (ZFC) and Field-cooling (FC) curves-

These are really two separate measurements and gives valuable information about a magnetic system when studied together.

The zero-field-cooled (ZFC) curve was taken by applying no field to the magnetic material while it was above its paramagnetic or superparamagnetic transition temperature. The sample was cooled to a low temperature, such as 5K while no field was applied. Then a small field such as 100Oe was applied and the magnetization of the sample was measured while it was brought back to room temperature, 300K. The field-cooled (FC) curve was taken by cooling the sample from above its paramagnetic or superparamagnetic temperature to a very low temperature, such as 5K, while in the presence of a small DC magnetic field, like 100Oe. The 100Oe field was maintained and the magnetization of the sample was measured while it was slowly heated back to room temperature (300K).

In order to extract useful information from this pair of curves, they must be measured with the same field strength. **Figure 2.1** represents a typical M-T curve at same field strength. When the two graphs are plotted on top of each other, there is a temperature at which they merge. This temperature is known as the irreversibility temperature (T_{irr}). The temperature at which the peak magnetization in the ZFC graph occurs is the blocking temperature (T_b). At T_b point, the thermal energy (k_BT) overcomes the anisotropy barrier. At any temperature above this, the thermal energy decreases the magnetization by randomizing the spin orientations.

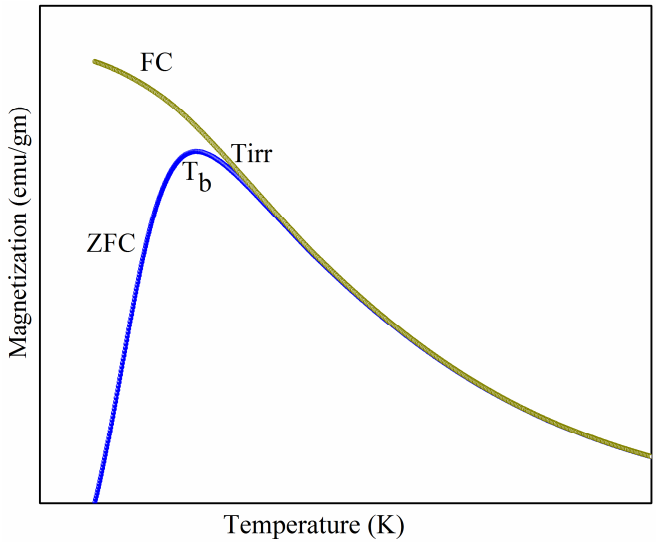

Figure 2.1 A typical ZFC and FC curve of magnetic nanosystem

This leads to a familiar Curie-Weiss law behavior ($M \propto 1/T - T_C$), where T_C is normally the Curie temperature.

b) Magnetization versus magnetic field

The Magnetization versus applied field curve typically abbreviated as M-H curve. The x-axis is the applied field (H) measured in Oersteds. The y-axis is the magnetization of the material measured in emu/g. When an external field is applied the plot moves to the right and up. As the strength of the magnetic field is increased, the slope begins to approach zero. This is the result of the fact that nearly all spins are aligned with the magnetic field and hence increasing the strength of the magnetic field has no effect. The magnetization at this point is called the saturation

magnetization (M_S) and is shown in **figure 2.2** as M_S. From this point the field strength is reduced. In a ferromagnetic material, the curve will not trace back upon itself. This property is known as hysteresis since the history of the sample determines its magnetic behavior. When the field is reduced back to zero, a net magnetization remains. This is known as the remanence magnetization (M_R) as shown in **figure 2.2.** M_R is an important property of applied magnetics because it determines how ñstrongò a magnet is. From this point, the field direction is reversed, reducing the magnetization eventually back to zero.

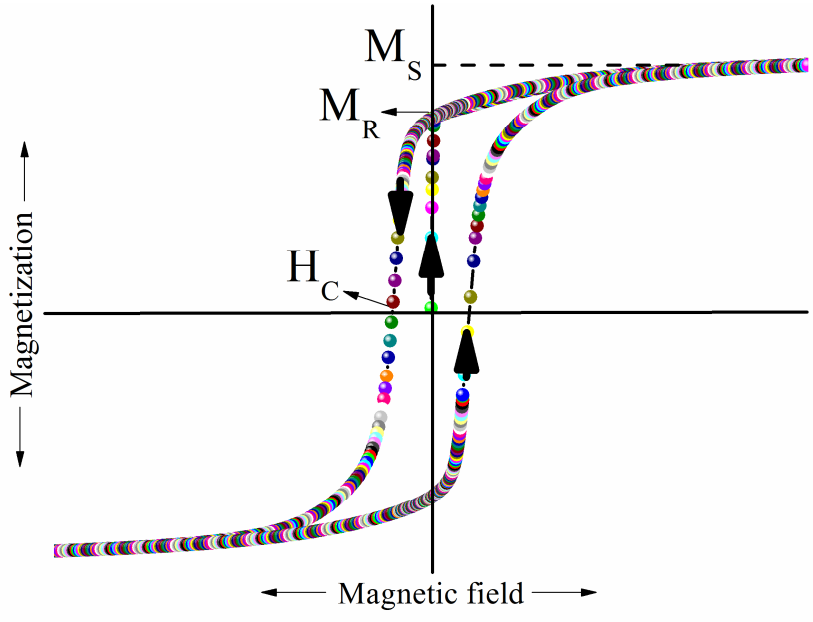

Figure 2.2 A typical ferromagnetic M-H curve

The field at which the magnetization goes back to zero is known as the coercivity of the material shown in **figure 2.2** as H_C. The coercivity can be thought of as how difficult the material is to demagnetize. In a typical ferromagnet, the bottom half of the curve is identical to the top half.

c) M-H Loops at different temperature

The various parameters of a magnetic material can be determined from temperature dependent M-H curve. An important material property for ferromagnets is the Curie temperature. The Curie temperature represents a first order transition from ferromagnetic to paramagnetic. At this temperature, the ordering length goes to

infinity and is seen as the susceptibility diverging to infinity for low fields. The coercivity of the material goes to zero. Zero coercivity would also imply zero remanence. This transition to a paramagnet is easily seen in a family of M-H curves taken at different temperatures. There is an analogous temperature for superparamagnetic particles called the blocking temperature. Below the blocking temperature the particles show nonzero coercivity and above the blocking temperature they act similar to a paramagnet with a large moment.

d) Hyperthermia

Hyperthermia thermal therapy or thermotherapy is a type of cancer treatment in which body tissue is exposed to high temperatures (up to 113°F). Research has shown that this high temperature can damage and kill cancer cells, usually with minimal injury to normal tissues. The most common MR imaging method used to measure temperature changes is the proton resonant frequency shift (PRFS) method. The PRFS method measures change in the temperature dependent proton resonance frequency of the water in tissue and uses it to calculate temperature change. Since, the MR image phase is a linear function of the frequency (at a fixed echo time-TE), a change in temperature results in a change in MR image phase, allowing temperature changes to be measured [35].

2.6 Conclusion

The characterization techniques discussed in this chapter spans over a wide range of categories. XRD and SAED pattern gives structural information about the sample. Size and shape of the nanosystems can be reliably determined from HR-TEM measurements. EDX measurements give compositional information of the nanosystems. FTIR provides information of the functional group present on the surface of the nanosystems while zeta potential provides surface potential which gives information about the stability of nanosystem in a solution. The UV, PL, and TRPL spectrophotometer provide absorption/emission pattern of the quantum dots and hybrid nanosystems. Using the PPMS, we can study the magnetic properties of the particles as a function of varying field strengths and temperatures. The sample concentration used for toxicity assay and for relaxivity measurement was calculated with the help of ICP-OES instrument. Fluorescence microscopy was used for the analysis of cellular uptake of nanosystem and

its fluorescence property at different excitation. The transverse relaxation time of the developed magnetic nanosystems was measured by using 14.1 T, Nuclear Magnetic Resonance (NMR) micro imager.

References:

[1] Xu, C. et al. A combined top-down bottom-up approach for introducing nanoparticle networks into nanoelectrode gaps. Nanotechnology **17**, (14), 3333--3339, 2006.

[2] Tang, L. et al. Bottom-up synthesis of large-scale graphene oxide nanosheets. *Journal of Materials Chemistry* **22**, (12), 5676--5683, 2012.

[3] Wang, Y. & Xia, Y. Bottom-up and top-down approaches to the synthesis of monodispersed spherical colloids of low melting-point metals. *Nano Lett.* **4,** (10), 2047--2050, 2004.

[4] Wong, T.-S., Brough, B. & Ho, C.-M. Creation of functional micro/nano systems through top-down and bottom-up approaches. *Mol. Cell. Biomech.* **6,** (1), 1--55, 2009.

[5] Amendola, V. *et al.* Top-down synthesis of multifunctional iron oxide nanoparticles for macrophage labelling and manipulation. *Journal of Materials Chemistry* **21,** (11), 3803--3813, 2011.

[6] Yu, W. W. *et al.* Synthesis of monodisperse iron oxide nanocrystals by thermal decomposition of iron carboxylate salts. *Chem. Commun. (Camb).* (20), 2306--2307, 2004.

[7] Langille, M. R. *et al.* Bottom-up synthesis of gold octahedra with tailorable hollow features. *J. Am. Chem. Soc.* **133,** (27), 10414--10417, 2011.

[8] Sinha, B., Müller, R. H. & Möschwitzer, J. P. Bottom-up approaches for preparing drug nanocrystals: Formulations and factors affecting particle size. *International Journal of Pharmaceutics* **453,** (1), 126--141, 2013.

[9] Lu, W. & Lieber, C. M. Nanoelectronics from the bottom up. *Nat. Mater.* **6,** (11), 841--850, 2007.

[10] Byrappa, K., Ohara, S. & Adschiri, T. Nanoparticles synthesis using supercritical fluid technology - towards biomedical applications. *Advanced Drug Delivery Reviews* **60,** (3), 299--327, 2008.

[11] Corchero, J. L. & Villaverde, A. Biomedical applications of distally controlled magnetic nanoparticles. *Trends in Biotechnology* **27,** (8), 468--476, 2009.

[12] Danhier, F. *et al.* PLGA-based nanoparticles: An overview of biomedical applications. *Journal of Controlled Release* **161,** (2), 505--522, 2012.

[13] Xie, J. *et al.* One-pot synthesis of monodisperse iron oxide nanoparticles for potential biomedical applications. *Pure Appl. Chem.* **78,** (5), 1003--1014, 2006.

[14] Thanh, N. T. K. & Green, L. A. W. Functionalisation of nanoparticles for biomedical applications. *Nano Today* **5,** (3), 213--230, 2010.

[15] Mourdikoudis, S. & Liz-Marzán, L. M. Oleylamine in nanoparticle synthesis. *Chemistry of Materials* **25,** (9), 1465--1476, 2013.

[16] Grzelczak, M. *et al.* Shape control in gold nanoparticle synthesis. *Chem. Soc. Rev.* **37,** (9), 1783ï 1791, 2008.

[17] Mousavand, T. *et al.* Organic-ligand-assisted supercritical hydrothermal synthesis of titanium oxide nanocrystals leading to perfectly dispersed titanium oxide nanoparticle in organic phase. *J. Nanoparticle Res.* **9,** (6), 1067--1071, 2007.

[18] Aryal, S., *et al.* Nanoparticle drug delivery enhances the cytotoxicity of hydrophobicï hydrophilic drug conjugates. *Journal of Materials Chemistry* **22,** (3), 994--999, 2012.

[19] Cong, H. & Porco, J. A. Chemical synthesis of complex molecules using nanoparticle catalysis. *ACS Catalysis* **2,** (1), 65--70, 2012.

[20] Sun, S. & Zeng, H. Size-controlled synthesis of magnetite nanoparticles. *J. Am. Chem. Soc.* **124,** 8204--8205, (28), 2002.

[21] De Palma, R. *et al.* Silane ligand exchange to make hydrophobic superparamagnetic nanoparticles water-dispersible. *Chem. Mater.* **19,** (7), 1821--1831, 2007.

[22] Zhang, T. *et al.* A general approach for transferring hydrophobic nanocrystals into water. *Nano Lett.* **7,** (10), 3203--3207, 2007.

[23] Saha, A. *et al.* Ligand exchange approach in deriving magnetic-fluorescent and magnetic-plasmonic hybrid nanoparticle. *Langmuir* **26,** (6), 4351--4356, 2010.

[24] Ko, Y. *et al.* Hydrophobic nanoparticle-based nanocomposite films using in situ ligand exchange layer-by-layer assembly and their nonvolatile memory applications. *ACS Nano* **7,** (1), 143--153, 2013.

[25] Dong, A. *et al.* A generalized ligand-exchange strategy enabling sequential surface functionalization of colloidal nanocrystals. *J. Am. Chem. Soc.* **133,** (4), 998--1006, 2011.

[26] Caragheorgheopol, A. & Chechik, V. Mechanistic aspects of ligand exchange in Au nanoparticles. *Phys. Chem. Chem. Phys.* **10,** (33), 5029--5041, 2008.

[27] Jha, D. K. *et al.* Simple synthesis of superparamagnetic magnetite nanoparticles as highly efficient contrast agent. *Mater. Lett.* **95,** 186--189, 2013.

[28] Yang, K. *et al.* One-pot synthesis of hydrophilic molecularly imprinted nanoparticles. *Macromolecules* **42,** (22), 8739--8746, 2009.

[29] Qi, L., Cölfen, H. & Antonietti, M. Synthesis and Characterization of CdS Nanoparticles Stabilized by Double-Hydrophilic Block Copolymers. *Nano Lett.* **1,** (2), 61--65, 2001.

[30] He, T. *et al.* Direct synthesis of anisotropic polymer nanoparticles. *Angew. Chemie - Int. Ed.* **46,** (48), 9243--9247, 2007.

[31] Marchegiani, G. *et al.* Sonochemical synthesis of versatile hydrophilic magnetite nanoparticles. *Ultrason. Sonochem.* **19,** (4), 877--882, 2012.

[32] Zhang, Y., Liang, X. & Li, L. Synthesis and photoluminescence properties of hydrophilic ZnS nanoparticles. *Mater. Lett.* **64,** (13), 1521--1523, 2010.

[33] Herranz, F. *et al.* A new method for the aqueous functionalization of superparamagnetic Fe2O3 nanoparticles. *Contrast Media Mol. Imaging* **3,** (6), 215--222, 2008.

[34] Qu, H., *et al.* One-pot synthesis in polyamines for preparation of water-soluble magnetite nanoparticles with amine surface reactivity. *Journal of Materials Chemistry* **22,** (8), 3311--3313, 2012.

[35] Wyatt. C., *et al.* Hyperthermia MRI Temperature Measurement: Evaluation of Measurement Stabilization Strategies for Extremity and Breast Tumors. *Int. J. Hyperthermia* **25**, (6), 422--433, 2009.